KcsA Crystal Structure as Framework for a Molecular Model of the Na^+ Channel Pore[†]

Gregory M. Lipkind[‡] and Harry A. Fozzard*[,§]

Cardiac Electrophysiology Labs, Departments of Biochemistry & Molecular Biology and Neurobiology, Pharmacology and Physiology, The University of Chicago, Chicago, Illinois 60637

Received March 2, 2000; Revised Manuscript Received April 26, 2000

ABSTRACT: The crystal structure of the pore-forming part of the KcsA bacterial K^+-selective channel suggests a possible motif for related voltage-gated channels. We examined the hypothesis that the spacial orientation of the KcsA M1 and M2 α-helices also predicts the backbone location of S5 and S6 helices of the voltage-gated Na^+ channel. That channel's P region structure is expected to be different because selectivity is determined by side-chain interactions rather than by main-chain carbonyls, and its outer vestibule accommodates relatively large toxin molecules, tetrodotoxin (TTX) and saxitoxin (STX), which interact with selectivity ring residues. The Na^+ channel P loop was well-modeled by the α-helix-turn-β-strand motif, which preserves the relationships for toxin interaction with the Na^+ channel found experimentally. This outer vestibule was docked into the extracellular part of the inverted teepee structure formed by the S5 and S6 helices that were spacially located by coordinates of the KcsA M1 and M2 helix main chains [Doyle et al. (1998) *Science 280*, 69−74], but populated with side chains of the respective S5 and S6 structures. van der Waals contacts were optimized with minimal adjustment of the S5, S6, and P loop structures, forming a densely packed pore structure. Nonregular external S5−P and P−S6 segments were not modeled here, except the P−S6 segment of domain II. The resulting selectivity region structure is consistent with Na^+ channel permeation properties, offering suggestions for the molecular processes involved in selectivity. The ability to construct a Na^+ channel pore model consistent with most of the available biophysical and mutational information suggests that the KcsA structural framework may be conserved in voltage-gated channels.

Voltage-gated K^+, Na^+, and Ca^{2+} channels belong to a structurally homologous superfamily of voltage-gated channels (*2*). Each channel-type is characterized by a highly selective permeability for specific ions. K^+ channels discriminate almost perfectly against Na^+ and Ca^{2+} under physiological conditions. Na^+ channels discriminate against Ca^{2+} and K^+ ions in ratios of at least 0.1. At physiological concentrations, Ca^{2+} channels exclude permeation by Na^+ and K^+, although they are permeable to monovalent cations at low divalent ion concentrations. All of the cloned voltage-gated channels share the common transmembrane topological motif of four homologous domains or subunits (I, II, III, and IV), each of which is composed of six transmembrane segments (S1−S6)[1] (*3*−*5*). The voltage-gated channels have characteristic S4 segments that contain positively charged amino acids at every third position, conferring their voltage sensitive property. On the basis of biophysical and biochemical data, the extracellular segment between S5 and S6 of each subunit or domain is proposed to fold back into the membrane to form the outside mouth of the pore and part of the ion-conducting pathway. This segment is called the P loop, and it includes the channel's selectivity filter (*6*).

Recently, MacKinnon and co-workers have solved at 3.2 Å resolution the pore structure of a bacterial K^+ channel named KcsA (*1*). This K^+ channel has the characteristic selectivity of voltage-gated K^+ channels, but it is not voltage dependent. The protein subunits contain only two membrane-spanning segments M1 and M2. Four subunits form a 4-fold symmetrical conducting pathway, lined by a "teepee" of converging M2 transmembrane helices. The P loops between the four sets of M1 and M2 α-helices are arranged together to form the selectivity filter of the channel, which is a 12 Å long and 3 Å diameter pore. In the P loop, the main-chain carbonyls of four highly conserved amino acid residues (TVGY of the signature sequence) face the pore, and their side chains face outward into the protein. This selectivity region structure was originally implied by mutational data (*7*), and the motif of five main-chain carbonyls facing the selectivity filter was also derived from structural modeling (*8*, *9*). In the KcsA crystal structure, the segment of the P loop immediately N-terminal to the strand that contains the selectivity sequence is an α-helix, resulting in a P loop with the motif of an α-helix-turn-nonregular extended strand.

[†] Supported by Grant PO1-HL20592 (H.A.F.) and a grant from the American Heart Association Midwest Affiliate (G.M.L.).

* To whom correspondence should be addressed.

[‡] Department of Biochemistry and Molecular Biology, The University of Chicago.

[§] Department of Neurobiology, Pharmacology, & Physiology.

[1] Abbreviations: S1−S6, the first through the sixth transmembrane segment of each of the four domains of the voltage-gated Na^+ channel; KcsA, K^+ channel from *Streptomyces lividans*; M1 and M2, the two transmembrane segments of the KcsA channel subunit; TTX, tetrodotoxin; STX saxitoxin; μ1, adult skeletal muscle Na^+ channel isoform.

10.1021/bi000486w CCC: $19.00
Published on Web 06/21/2000

Structural and experimental evidence favor the idea that the KcsA channel is an evolutionary predecessor of the six-transmembrane segment family of voltage-gated K^+ channels (*10*, *11*). The M2 α-helices of the four KcsA P subunits, which would correspond to the S6 segments in voltage-gated K^+ channels, form the central pore with an inverted teepee or cone structure. The pore α-helices that precede the selectivity filter signature sequence in the P loops are positioned between M2 helices of neighboring subunits. The outer M1 α-helices, corresponding to S5 of the voltage-gated channels, face the lipid phase of the membrane. Dense packing of the helices and the P loops provides the nonbonded contacts that hold the tetramer together. An important structural feature of the P loop is that it confers rigidity to the channel's selectivity region.

It is likely that voltage-gated Na^+ channels have evolved from K^+ channels by gene duplication (*12*), suggesting the intriguing possibility that some general features of their transmembrane helical structures may be similar. However, to account for their different permeation and selectivity properties, the outer vestibules of the pores and the selectivity filters must obviously be different. For the Na^+ channel, the side chains of a restricted number of amino acid residues, instead of main-chain carbonyls, form the selectivity filter (*13*−*18*). Specifically, a series of point mutations in P loops of Na^+ channels identified residues intimately related to sodium conductance, selectivity, and interaction with the pore-blocking guanidinium toxins, TTX and STX. Amino acid homology alignment distinguishes a cluster of four highly conserved amino acids in the same relative positions in the P loops of domains I−IV that participate in the formation of the selectivity filter—Asp-400, Glu-755, Lys-1237, and Ala-1529 (DEKA motif) (numbers of the μ1 adult skeletal muscle channel). Other nearby residues have also been reported to influence selectivity more modestly (*19*, *20*).

It has been difficult experimentally to resolve the molecular interactions responsible for selectivity (*16*, *21*). Analysis of the molecular basis for permeation and selectivity of the voltage-gated Na^+ channels would benefit from crystal structures of the appropriate regions. However, because of their size and less symmetrical structure, it is unlikely that such crystal structures will be available soon. Molecular models based on primary structure, rules of protein secondary structure, and intuition from biophysical studies have yielded important insights into channel structure and helped to guide experimental studies (*6*, *9*, *22*). We previously described a molecular model of the outer vestibule of the Na^+ channel that was formed by the binding surfaces for TTX and STX, which are small, structurally defined pore-occluding toxins (*23*). This model was based on site-directed mutagenesis data (*13*, *24*) and the structures of the guanidinium toxins (*25*). It consisted of four 10-amino acid segments, one from each of the four P loops. Our predicted P loop secondary structure was β-hairpins, based on protein structural rules (*26*). These were not arranged as a β-barrel, but radially, with the C-ends forming the inner walls of the pore and the N-ends outside to face the protein. These four P loops partially traversed the membrane and created at the bottom of the vestibule a narrow region formed by the side chains of the DEKA residues. The shape of the modeled vestibule was roughly conical, with a wide outer opening about 10−12 Å in diameter, corresponding to the sizes of TTX and STX. The outer opening of the vestibule must be this wide because the toxins enter the vestibule and interact directly with several of the selectivity ring residues within the vestibule (*13*, *17*). The P loops were arranged in a clockwise pattern, although the alternative counterclockwise pattern has also been proposed (*9*, *27*, *28*). The basis for the clockwise choice is 2-fold. First, this arrangement is most compatible with docking of the guanidinium toxins (*17*). Second, contact points between amino acids residues of μ-conotoxin, which is a 22-amino acid peptide toxin, and the outer ring of residues of the Na^+ channel outer vestibule (Glu-403, Glu-758, Asp-1532, and Met-1240) according to mutant cycle analysis are most consistent with the clockwise arrangement of the four domains (*29*).

The structural motif for the C-terminal part of P loops of domains I−IV of the Na^+ channel in our original model is in accordance with the pattern of fractional electrical distances into the membrane field that were determined by the voltage dependence of Cd^{2+} block of cysteine-substituted mutants in corresponding positions (*30*−*32*). The proposal that the DEKA selectivity filter residues are part of a turn and change of direction of the P loops proposed in our model has been supported experimentally. The amino acid residue positions in the C-terminal parts of all of the P segments are deepest in the electric field for the DEKA selectivity filter residues (e.g., 0.32 for Asp-400), and this depth decreases monotonically toward the C-terminus, as in our original model in which these segments were β-strands (*23*). The residues of the vestibule's external charged ring—Glu-403, Glu-758, Asp-1241, and Asp-1532 demonstrate only shallow voltage dependence, consistent with their more superficial location. Cysteine substitutions of the N-terminal parts of the P loops show either no Cd^{2+} or methanesulfonate block from inside or outside or are more shallow than the DEKA ring, implying that they are removed from the pore or are partially buried in the protein (*32*). However, these results for the N-end segments of the P loops preceding the selectivity filter provide no direct structural insight into its secondary structure.

We originally proposed β-hairpins for the secondary structure of the P loops because they provided us with stable structures for docking of the pore-blocking toxins in the molecular model. However, another plausible alternative for the secondary structures of both Na^+ and Ca^{2+} channel P loops is the α-helix-turn-β-strand motif ($\alpha\beta$ arches) (*33*), which would be more consistent with the P loop motif of the KcsA channel (*1*). Given their probable common ancestry, it is likely that the voltage-gated channels have a similar arrangement of their P loops, as originally proposed on structural grounds by Guy and Conti (*6*). Here we examine the implications for Na^+ channel pore structure of using the α-helix-extended strand motif for the P loop and the KcsA channel teepee structure for the S5 and S6 transmembrane segments. The S5−S6 segments vary substantially in length between domains, and somewhat less between isoforms. The domain I S5−S6 segment is longest (>100 residues) and contains consensus glycosylation sites. The domain II S5−S6 is the shortest, with 53 residues (*34*). The P loops are a small, quite conserved part of the entire S5−S6 segments, and we consider 24 residues from each domain as the P loops. The less homologous S5−S6 segments outside the P

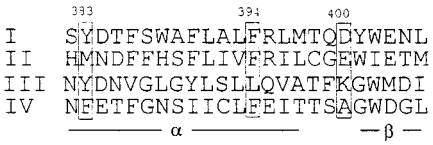

FIGURE 1: Alignment of amino acid sequences of P loops of domains I−IV of the Na^+ channel (μ1 isoform). The numbering corresponds to the P loop of domain I. Residues of the selectivity filter DEKA motif are enclosed in a box. Two other highly conserved residue locations are also highlighted. At the bottom, the bar labeled α represents the proposed α-helical region, and β represents the β-strand region.

loops were not included in the model because of lack of experimental constraints on their structures, except for domain II P−S6 segment, for which some data are available (see later). P loops were aligned and organized into the α-helix-turn-β-strand structures, with the β-strands facing the pore. The four P loops were assembled radially with the same relationship of the C-terminal β-strands that was required for formation of the guanidinium toxin sites (*23*). The P loop backbone motifs were assumed to have 4-fold symmetry, despite the specific residue differences between the domains. The S5 and S6 segments were aligned and the backbones were assigned the identical coordinates as the M1 and M2 segments of the KcsA channel. The P loops were then added to the inverted teepee structures of transmembrane segments organized in a clockwise pattern, permitting dense packing of the amino acid residues. This procedure allowed us to reconstruct a closed model of the outer vestibule of the Na^+ channel with P loops of domains I−IV inside and transmembrane segments S5 and S6 outside. The model predicts the spacial relationship between the residues of Na^+ channel that are known to be critical for selectivity and permeation, for comparison with its sieving properties and the experimental studies of selectivity alteration by mutation.

MATERIALS AND METHODS

Modeling was accomplished in the Insight and Discover graphical environment (Biosym Technologies, Inc., San Diego, CA) as previously described (*23*). Energetic calculations utilized the consistent valence force field approximation. For minimization procedures, the steepest descents and conjugate gradients were used. Because much of the mutational data are from the adult skeletal muscle isoform (μ1) of the Na^+ channel, residue modeling and the residue numbering will be according to that isoform. The regions modeled are highly homologous, and any isoform differences will be noted.

RESULTS AND DISCUSSION

P Loops. Alignment of the P loop amino acid sequences of Na^+ channels (*5*) by the putative selectivity filter residues shows that they contain a region of highly conserved hydrophobic residues just N-terminal to the selectivity filter (Figure 1). For domain I, these correspond to residues 386-394. Noteworthy are the Phe-394 and Phe or Tyr-383 residues in two positions and the Trp-402, which are conserved in the other domains and adjacent to charged or hydrophilic residues, reflecting unique structural similarities between domains. These residues are highly conserved in mammalian and invertebrate isoforms. Among the 17 isoforms summarized by Goldin (*5*), position 394 and its equivalent in the other domains has only phenylalanine or in a few cases leucine, and position 402 and its equivalents has only tryptophan, except for a proline in the unusual second heart isoform that has never been expressed. The hydrophobic character of these sequences N-terminal to the selectivity filter residues and the high proportion of α-helical forming residues (Ala, Leu, Phe, and Met) (*26*, *35*) encourages their modeling as α-helices (*9*, *36*). Moreover, the preference of Asp, Glu, and Asn for the N-terminus and Arg, Lys, and Gln for the C-terminus of α-helices allows their extension to 382−397. The first question is does this α-helix-turn-strand motif form an appropriate structure for the P loops of the voltage-gated Na^+ channel?

The α-helix-turn-β-strand motif is a common type of structural organization, with a hydrophobic residue on one side of the β-strand fitting into a hydrophobic pocket in the α-helix (*33*, *37*). In this motif, two interacting bulky hydrophobic residues (usually Leu, Val, Ile, or Phe) are well conserved—the first is inside the last turn of the α-helix and the second is at the beginning of the β-strand in the second position. An example of such a polypeptide sequence is positions 55−74 in nuclease (*38*) with interaction between the α-helix Val-66 with Ile-72 of the β-strand. In αβ-arches with short turns, these hydrophobic residues usually occupy the first and seventh positions in the amino acid sequences. Unexpectedly, there is a tendency for Gly residues in the αβ-fragments to be located not only in turns, but also preceding a bulky hydrophobic residue inside the β-strands (Gly-228 before Trp-229 in triose phosphate isomerase (*39*) (see also Table 2 in ref *37*). The residues between the α-helices and the β-strands (Thr-398, Gln-399, and Asp-400 in domain I) form the turn region of the P loops. Although β-strands of αβ motifs often participate in formation of β-sheets or β-barrels, as in the case of triose phosphate isomerase (*39*), they often exist as single extended strands. One such example is an external β-strand of the B-chain of insulin (B24−B28), interacting with the preceding α-helix (B9−B19) (*40*).

In the proposed α-helix-turn-β-strand model for P loops, the first residues on the N-terminal sections of the extended segments facing the pore are the selectivity filter residues (which also participate in formation of the turns). Then, there is a conserved Trp in the second position of each β-strand (e.g., Trp-402 of domain I), except for domain II, where the analogous residue is Ile. The αβ-structure 55−74 of nuclease resembles the conformation of P loops of the KcsA channel, with the relatively tilted arrangement of the N-terminal α-helix (*1*). Using it as a template, we configured the P loops with the β-strand Trp residues interacting with bulky hydrophobic residues in the appropriate positions of the α-helices (Leu-396 in domain I of μ1, and Val, Ile, Cys in the other domains). This hydrophobic interaction stabilizes the αβ structure of the P loops. The optimized structure of the P loop of domain I of the Na^+ channel is shown in Figure 2. Here, the inner hydrophobic core is formed by the side chains of amino acid residues Leu-396, Gln-399, and Trp-402. Substitution of these hydrophobic residues by hydrophilic ones would be expected to destabilize the vestibule above the selectivity filter.

It is essential that any model of the Na^+ channel vestibule retain an energetically correct binding site for the guani-

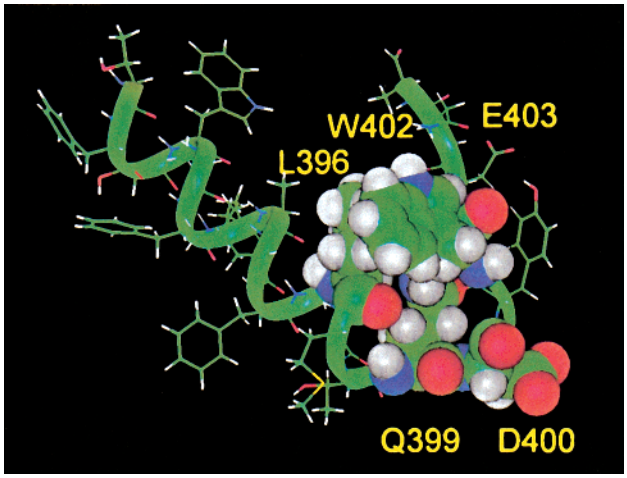

FIGURE 2: The α-helix-turn-β-strand conformation of the Na^+ channel domain I P loop. The inner hydrophobic core that stabilizes the structure is formed by the side chains of amino acid residues Leu-396, Gln-399, and Trp-402, which are shown by space-filling images.

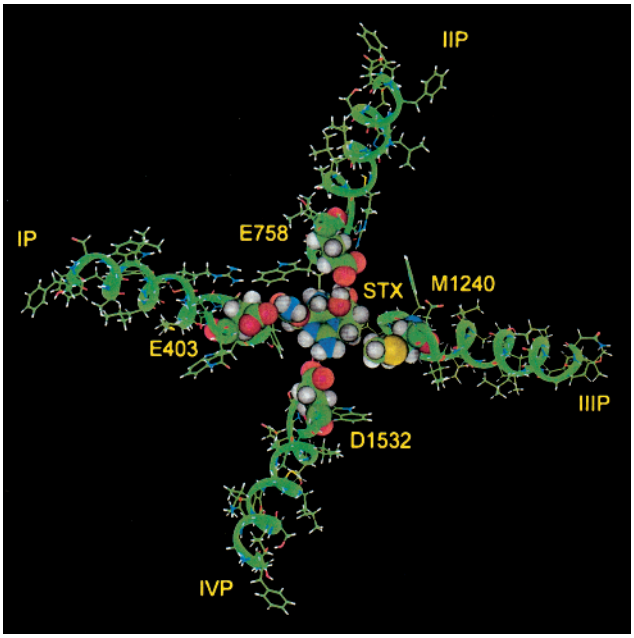

FIGURE 3: Arrangement of α-helix-turn-β-strand motifs of the Na^+ channel P loops of domains I−IV, shown by green ribbons, in a clockwise manner to form the TTX/STX binding site. STX and some interacting residues are shown by space-filling images. Note that in this model the P loops are not in van der Waals contact with each other, and could maintain this arrangement only if supported by other parts of the channel protein.

dinium toxins. Assembly of the four Na^+ channel P loop αβ-hairpins to form the guanidinium toxins binding pocket is shown in Figure 3. In the previously used β-hairpin model, the glycines were located in the turns, but the new turns in domains III and IV locate them next to the bulky hydrophobic Trp residues. The new model presents a symmetrical model of the TTX/STX-binding site, with the β-strands of the αβ-structures located toward the central axis and the α-helices located outside the pore. The alternation of direction of side chains in the β-strands are most consistent with known interactions of these stretches with TTX and STX (*13*, *17*, *23*); alternative nonregular patterns for these segments result either in loss of the toxin interactions or loss of stability of the αβ structure or both. The retained interactions with the guanidinium toxins include the following features (*17*, *23*):

(1) The 7,8,9 guanidinium group of STX and the 1,2,3 guanidinium group of TTX are directed into the pore, where they interact most strongly with Glu-755 of domain II and Asp-400 of domain I.

(2) The 1,2,3 guanidinium group of STX, which is located at right angles to the planes of the 7,8,9 guanidinium in the rigid STX structure, interacts with Asp-1532 of domain IV.

(3) In the plane of the 1,2,3 guanidinium group on the opposite side of the STX molecule is a C-12 *gem*-diol, postulated to interact with Glu-758 of domain II.

(4) There is a strong nonbonded interaction between the aromatic ring of Tyr-401 of domain I and the nonpolar surface of TTX.

A consequence of the wide separation of the P loops that is necessary to accommodate STX and TTX is that the P loops fail to have interdomain van der Waals contacts (Figure 3), in contrast to the closely packed P loops of the KcsA channel. For the vestibule structure to be maintained without mutual interactions between P loops, it must be stabilized by nonbonded contacts with some other parts of the protein. One possibility for occupancy of the space between P loops is the upper parts of S6 segments, which have themselves been implicated in pore behavior (see below).

S5 and S6 Alignment. The M1 and M2 helices of the KcsA channel form an inverted conical "teepee". In accordance with the idea that the KcsA channel is analogous to the pore part of the Na^+ channel, we considered the hypothesis that the S5 and S6 helices are equivalent to the M1 and M2 helices. To test this construction, it is first necessary to determine an alignment of the S6 amino acids with those of M2. Doyle et al. (*1*) found that the N-terminal Trp-87 residues of the M2 helices play an important part in the helical arrangement within the membrane. Therefore, our initial step was to align the conserved bulky hydrophobic residues on the N-ends of the S6 helices with the Trp residue of KcsA (Figure 4). This alignment results in considerable homology of amino acids of domains I−IV. In the case of domain IV S6 of μ1, the corresponding residue is Ile-1566, while for S6's of domains I, II, and III, the residues are Tyr-417, Met-771, and Tyr-1263. Two aromatic residues in the middle of domain IV S6 (Phe-1764 and Tyr-1771 of the brain2 channel, or Phe-1579 and Tyr-1586 of μ1) have been proposed to interact with local anesthetic drugs within the pore (*41*, *42*). This alignment places them in the corresponding pore-facing positions of Ile-100 and Thr-107 of KcsA. This alignment also directs the side chains of residues Asn-434 and Leu-437 of domain I S6 into the pore, in accordance with the report of Wang and Wang (*43*) that mutations to Lys at these sites affected the local anesthetic block of the Na^+ channel. These residues guiding the orientation of S6 α-helices are highly conserved in mammalian and invertebrate isoforms of the channel. The proposed alignment of S6 residues can be further tested by substitution of these residues by cysteine and determination of their orientation toward the water-filled pore by reaction with methansulfonate reagents. The alignment also suggests possible additional interaction sites for local anesthetics.

No direct experimental evidence is available to assist in alignment of S5 segments. The C-ends of the S5 helices have highly conserved Phe residues (Squid and *Drosophila* have

KcsA	I	II	III	IV
Trp-87	Tyr	Met	Tyr	Ile-1566
Gly	Met	Cys	Met	Gly
Arg	Ile	Leu	Tyr	Ile
Leu	Phe	Thr	Leu	Cys
Val	Phe	Val	Tyr	Phe
Ala	Val	Phe	Phe	Phe
Val	Val	Leu	Val	Cys
Val	Ile	Met	Ile	Ser
Val	Ile	Val	Phe	Tyr
Met-96	Phe	Met	Ile	Ile-1575
Val	Leu	Val	Ile	Ile
Ala	Gly	Ile	Phe	Ile
Gly	Ser	Gly	Gly	Ser
Ile-100	Phe	Asn	Ser	Phe-1579
Thr	Tyr	Leu	Phe	Leu
Ser	Leu	Val	Phe	Ile
Phe	Ile	Val	Thr	Val
Gly	Asn-434	Leu	Leu	Val
Leu	Leu	Asn	Asn	Asn
Val	Ile	Leu	Leu	Met
Thr-107	Leu-437	Phe	Phe	Tyr-1586
Ala	Ala	Leu	Ile	Ile
Ala	Val	Ala	Gly	Ala
Leu	Val	Leu	Val	Ile
Ala	Ala	Leu	Ile	Ile
Thr	Met	Leu	Ile	Leu

FIGURE 4: Proposed alignment of S6 segments of domains I−IV of the Na^+ (μ1 isoform) channel with M2 of the KcsA channel. Some residues with the side chains facing the pore are enclosed in boxes. Some of the pore-facing residues in domains I and IV were predicted on the basis of local anesthetic drug interactions within the pore.

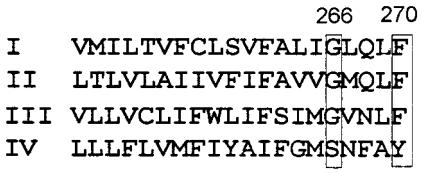

FIGURE 5: Alignment of amino acid sequences of S5 segments of domains I−IV of Na^+ channels (μ1 isoform). The conserved portions are highlighted. The conserved small G/S residues establish interaction between the C-ends of S5 and the N-ends of S6 α-helices.

Tyr in domain I) and four residues proximal in each domain is a very conserved Gly (Figure 5). We assumed that these conserved Gly residues inside the C-terminus play a structural role in docking the C-ends of S5 helices with the bulky hydrophobic residues on the N-ends of S6 helices to form the teepee structure. Consequently, these Gly residues were placed at the interfaces with bulky hydrophobic residues of the S6 α-helices to form the inverted teepee motif for S5 and S6 with the identical spacial coordinates of the M1 and M2 backbones. For example, the Gly of domain III S5 interacts with Tyr-1265 of S6 in this model. The interactions between S5 and S6 residues were similar to those between M1 and M2, despite changes in residues. Alternative orientations of the S5 helices are possible, but this proposed alignment provides a hypothesis that can be tested experimentally by using simultaneous mutations of these Gly residues and the corresponding bulky residues on the N-ends of S6 α-helices.

Docking of the Na^+ Channel Vestibule Structure with the S5−S6 Teepee. In the KcsA structure, the P loop α-helices are intercalated at an angle between the outer segments of

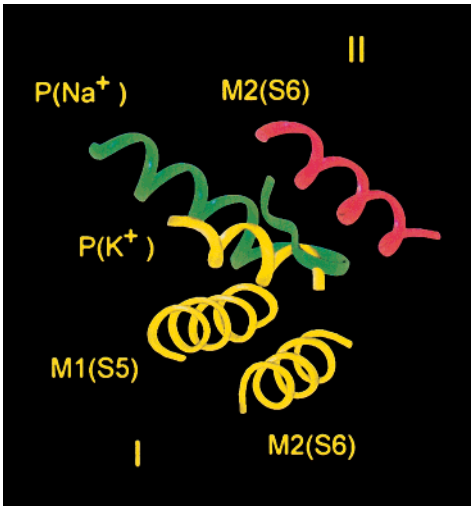

FIGURE 6: Superposition of the Na^+ channel P loop (green ribbon) on the KcsA P loop and neighboring M1 (S5) and M2 (S6) transmembrane helices. The P loop of one KcsA subunit and the corresponding M1(S5) and M2(S6) are shown by the yellow ribbon, and a segment of the adjacent domain is shown by the red ribbon. Because of the need of the Na^+ channel vestibule to accommodate TTX and STX, its P loop is displaced away from the center of the pore and its β-segment is spacially in the location of the KcsA P loop α-helix.

the M2 helix teepee, while the nonregular extended P loop C-terminal sections are densely packed to form a long narrow (∼3 Å diameter) selectivity region (*1*). However, the outer mouth of the Na^+ channel vestibule is much wider (∼12 Å diameter) than that of the KcsA channel because of the need for it to accommodate the large TTX and STX molecules between the P loop side chains (*13*, *17*) and because Zn^{2+} interacting with Cys-401 leaves enough room for Na^+ permeation (*24*). Initial superposition of the P loops of this wide funnel-shaped Na^+ channel vestibule with the KcsA channel P loops, relative to the same central axis, showed that the Na^+ channel P loop β-strands are necessarily more distant from the pore axis, almost occupying the space of the α-helices of the KcsA P loop. This displaces the α-helices of the Na^+ channel P loops away from the pore, where they are in contact with the S5 α-helices. This is the only way to locate these α-helices farther from the center axis of the pore in the space between S5 and S6 segments without significantly changing the S5 and S6 spacial coordinates from those of the M1 and M2 teepee (Figure 6). This specific location of the P loop α-helices also determines orientation relative to the pore of the turns and location of β-strands of the rigid frame of the four P loops inside the teepee (Figure 3). To determine the approximate depth of the outer vestibule of the Na^+ channel within the teepee, on the next docking step the framework of β-strands and neighboring turns alone, without the P loop α-helices, were lowered one by one into the inverted teepee composed of the S5 and S6 α-helices of four domains. The alignment of the β-strand framework to the center axis of the pore to intercalate them between the S6 helices was retained, while maintaining an approximately planar relation between the turns. Each P loop fragment was placed clockwise to its S6, viewed from the outside, according to the relationship found in the KcsA crystal structure. These fragments formed van der Waals contacts with the narrowing walls of the S6 teepees approximately at the level of Ile-1575 from domain IV S6. Consequently,

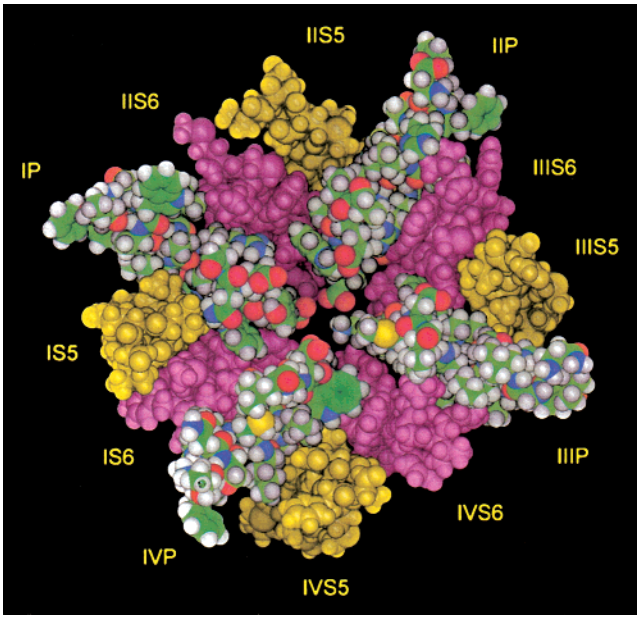

FIGURE 7: Model of the outer vestibule of the Na^+ channel (μ1 isoform) shown by space filling images. The model includes α-β-units of P loops with regular colors of the atoms and α-helices of S5 (yellow balls) and S6 (pink balls) segments of domains I−IV in a clockwise arrangement. Note that the P loops are intercalated between the S6 segments of the four domains, with the P loop α-helix also in contact with S5 of its own domain.

this S6 level determined the subsequent arrangement of the P loop α-helices, which can be located only laterally between the S5 and S6 helices of the same domains and the S6 helices of the neighboring domains.

Packing of each Na^+ channel P loop (domain I is illustrated in Figure 6) into the space between the S5 and S6 helices of the same domain and S6 of the neighboring domain was accomplished by adjustment of the location and conformation of the residue side chains of the P loop α-helices as well as the S5 and S6 of neighboring segments to avoid the more obvious van der Waals conflicts. The potential energy of nonbonded interactions for each set of S5−S6−P loop-S6 was minimized independently. The S6 main-chain helical coordinates required no adjustment because of the good fit, but the S5 helices were minimally displaced outward by their additional interactions with the P loop α-helices. As a result, the P loop α-helices formed a densely packed contact with α-helices of S5 and S6 segments of their domain and S6 of the neighboring domain. The domains were arranged clockwise, as supported by our studies of the interactions of the guanidinium toxins (*17*) and μ-conotoxin (*44*). The four optimized assemblies, including a P loop and the S5 and S6 helices from one domain and the S6 helix from an adjacent domain were combined on the basis of superposition of their S6 α-helices with corresponding backbones of S6 α-helices of the initial teepee model that was formed using the backbone coordinates of the M2 helices of the KcsA crystal structure. Then minimization of the potential energy of nonbonded interactions was made, determining the optimal arrangement of the four domain assembly (Figure 7). Although the initial docking was made with the P loop turns planar, the additional constraints of the symmetrical S6 teepee were such that there was little opportunity for displacement vertically of any of the α-helices and turns.

This procedure now resulted in a closed model of the outer vestibule of the μ1 Na^+ channel outer vestibule (Figure 7). The dense packing of the P loops between the S5 and S6 helices provided structural stability of the selectivity region at the P loop turn without requiring alteration of the spacial relationships between the DEKA selectivity residues. The surface of the outer vestibule was formed by β-strands of the four P loops, as in our initial model (*23*). The P loop β-strands were held in position by their interaction with the P loop α-helices, which were themselves held in position by their S5−S6 interactions. Note again that this differs from the densely packed arrangement of the P loops of the KcsA channel (*1*). In this modeled structure (Figure 7), the P loops do not form immediate steric contacts. Rather, one residue from each S6 is intercalated between each pair of side chains on the level of the selectivity DEKA residues. However, there is little room for backbone flexibility inside the α-helix-turn-β-strand P loop motifs in this native Na^+ channel outer vestibule structure. The least constrained residues are those of the outer charged ring, which are fixed only by hydrophobic interactions between neighboring Trp or Ile and the P loop α-helices. Presumably, they are also in contact with residues of the P−S6 segments not modeled here (but see below). Stereochemically different substitutions in the αβ hydrophobic pocket, such as mutation from Trp to Cys, would be expected to result in local conformational flexibility of the β-strands of the P loops. Backbone flexibility of the P loops has been suggested by double Cys mutants in the C-ends of the P loops, with formation of disulfide bonds (*20*, *45*, *46*) between residues that in our model exceed typical distances for disulfide formation. Those results are expected to be a consequence of disruption of the inner hydrophobic interactions of the α-helix-turn-strand structure, when the critical Trp residues are replaced with Cys.

To maintain the spacial relationships of the P loop β-strand residues known to interact with the guanidinium toxins as we previously modeled them (*17*, *23*), it was necessary that the β-strands not move significantly in either the vertical or the horizontal directions, despite different amino acids in both the P loops and the S5 and S6 helices between the domains. However, experimental studies have suggested that the selectivity filter DEKA residues may not be at exactly the same depth within the pore (*31*, *32*). When these selectivity filter residues are replaced by Cys, they form Cd^{2+}-binding sites, allowing the voltage dependence of Cd^{2+} block and, thereby, estimation of the fraction of the membrane field seen at the level of the substituted Cys residue SH group. The selectivity filter residue Asp-400 is thereby estimated to be 32% into the field, Lys-1237 is at 25%, and Ala-1529 is at 37%. The outer ring residues are also reported to be at slightly different fractions of the membrane field: Glu-403 is at 13%, Glu-758 is at 8%, Met-1240 to be at 10%, and Asp-1532 to be at 16%. Translation of these electrical measurements into physical distances is uncertain, because of possible nonuniformities of the electric field in the pore and its distortion by mutations. Furthermore formation of the DEKA selectivity filter most likely requires that the residues be arranged adjacent to each other. Nevertheless, these experimental data do raise the possibility that the P loops are not quite as symmetrical as presented here. A model based on the Cd^{2+} field depth data has been proposed, consisting of four nonregular structures for the P loop C-ends

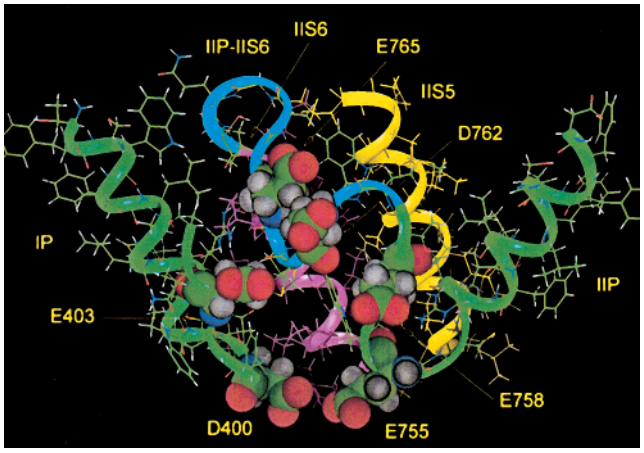

FIGURE 8: Possible arrangement of the short domain II P−S6 linker (blue ribbon). Side view also presents domains I and II P loops (green ribbons) and the enclosed domain II S5 (yellow ribbon) and domain II S6 (pink ribbon). Space-filling images are the four P loop residues involved in TTX/STX binding (Asp-400, Glu-403, Glu-755, Glu-758) and the two charged residues in the P−S6 linker (Asp-762 and Glu-765). This arrangement buries the top of the S6 α-helix with the P−S6 loop, and exposes two charged residues near the vestibule's outer ring of charged residues, where they might interact with vestibule blocking molecules.

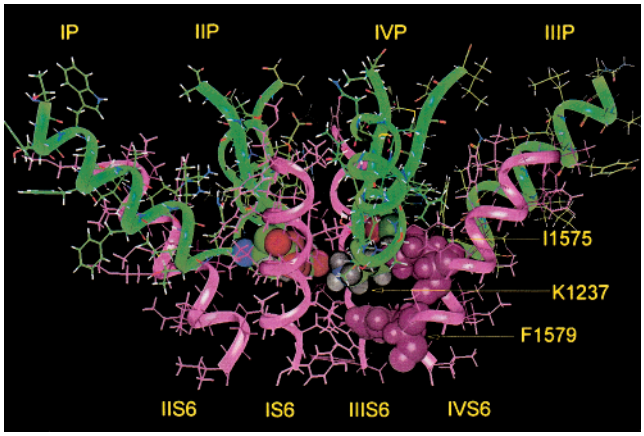

FIGURE 9: Side view of the arrangement of P loops (green ribbons) inside the teepee that is formed by S6 α-helices (pink ribbons). Amino acid residues of the selectivity filter and Ile-1575 and Phe-1579 of domain IV S6 are shown by space-filling images. Beneath the selectivity filter is a relatively wide region of the pore, sufficient for a local anesthetic molecule to interact with Phe-1579 and locating it about 9 Å from the selectivity filter lysine residue. Ile-1575 is just above Phe-1579 and at the level of the selectivity filter.

(*46*). Because of its asymmetry, it was not feasible to dock that vestibule model into the S5,S6 teepee.

The outside ends of the S6 helices, marked by pink in Figure 7 are located behind the P loops. Although in this view, the S6 α-helices appear to be on the protein surface, the loops connecting the C-ends of the P loops to the S6 helices must lie on top of the S6 helices, screening them from the outside. These P−S6 connectors therefore could form the more superficial walls of the outer vestibule, and they may contribute to the interactive site for μ-conotoxin. Neutralization of charged residues Asp-762 and Glu-765 in the domain II P−S6 have been reported to have a large effect on μ-conotoxin block (*47*) (but see ref *48*). They are unlikely to have much effect on TTX and STX, which bind deeper into the vestibule (*17*, *23*). A speculative reconstruction of the conformation of the P−S6 segment of domain II is proposed in Figure 8. This arrangement places Asp-762 and Glu-765 on the vestibule surface between and just exterior to Glu-403 and Glu-758 locating μ-conotoxin inside the pore (see ref *44*). Models of the other P−S6 segments were not attempted here because of their greater length and the paucity of experimental data.

In this model, the S6 segments have immediate contact with the selectivity filter residues. The domain IV S6 residue one helical turn above Phe-1579 is Ile-1575, which is located by the energy minimization procedure at the level of the selectivity filter between the side chains of Lys-1237 and Ala-1529. Ile-1575 has been connected experimentally to the selectivity process. Its mutation to Ala creates an access path for the membrane impermeable lidocaine derivative QX molecules through the pore (*41*, *49*−*51*). The side view of the P loop docking with the S6 teepee highlights the relationship of two amino acids of the Na^+ channel domain IV S6—Ile-1575 and Phe-1579, as shown in Figure 9. Phe-1579 of the μ1 Na^+ channel corresponds to Phe-1764 of the rat brain2 channel, and both of these highly conserved residues are thought to interact directly with local anesthetic drugs that typically access their site from the inside of the membrane (*41*, *42*). Figure 9 illustrates that the docking procedure placed the side chain of Phe-1579 below the selectivity filter and in proximity to the selectivity ring Lys-1237 of domain III. The location of domain IV S6 between the P loops of domains III and IV was a consequence of the relationship of the P loops to the transmembrane helices of the KcsA channel and our clockwise domain arrangement. This relationship is also supported by the experimental demonstration of an electrostatic interaction between Lys-1237 and the local anesthetic drugs, and the absence of such interaction with Asp-400 and Glu-755 of the selectivity filter (*42*). Lys-1237 is located in the model at a distance of about 9 Å from the local anesthetic site. As seen in the KcsA crystal structure, the pore region immediately inside the selectivity filter is sufficiently large to contain local anesthetic molecules in a water environment.

In this examination of the suitability of the M1 and M2 teepee structure of the KcsA channel for organization of the Na^+ channel pore, we have not considered the inner third of the pore. In the KcsA structure the transmembrane helices overlap to create a small inner vestibule opening (*1*), and the suggestion has been made that this region might be involved in activation gating (*52*). However, there is evidence that the S6 helices of the Shaker K^+ channel are sharply tilted outward (*53*). Because of the lack of experimental information about the inner third of the Na^+ channel S6 segments and the likelihood that they may also be tilted, it was premature to model that part of the pore.

Speculation on Mechanism of Selectivity of the Na^+ Channel Based on This Model. It has long been believed that selectivity involves interaction of the permeating Na^+ with one or more carboxyl residue (*2*). Furthermore, at physiological concentrations, the Na^+ channel behaves like a single ion pore, although at molar concentrations there may be a second Na^+ binding site (*27*). This means that usually only one Na^+ ion interacts with the critical narrow region at a time (*2*). Evidence that the DEKA ring is a key part of the selectivity filter of the Na^+ channel has been thoroughly reviewed by Favre et al. (*15*). Figure 10 illustrates the detailed relationships within the Na^+ channel DEKA selec-

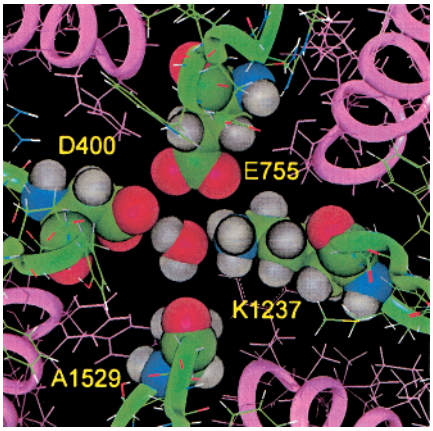

FIGURE 10: The selectivity filter of the Na^+ channel (μ1), with residues of the DEKA motif shown by space-filling images. The side chains of Glu-755 and Lys-1237 of domains II and III are located at a distance compatible with a salt bridge interaction. The side chains of Asp-400 of domain I and Lys-1237 are separated by one molecule of water, which is shown in the center of the figure. The open area inside of the pore is about 3 × 5 Å (in the absence of water), and there is room for the side chain of Lys-1237 to move toward Ala-1529.

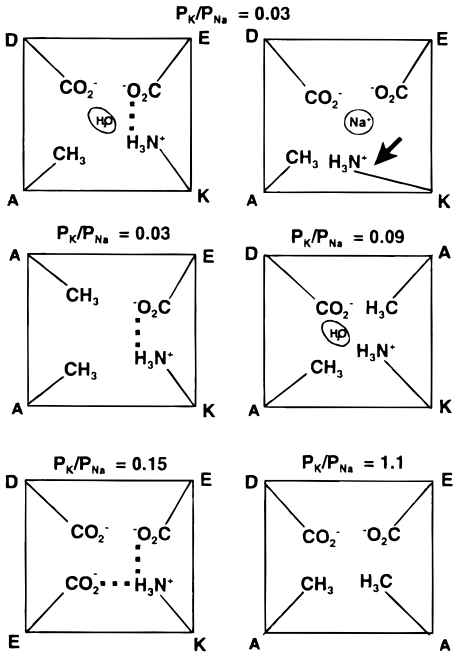

FIGURE 11: Conformational states and possible intramolecular interactions inside of the selectivity filter of the Na^+ channel and its mutants. Possible substitutions inside of the DEKA motif are shown on corners of the squares. The permeability ratios indicated for each schematic have been determined experimentally for the substitutions shown at the corners of the squares (*15*), except for the DEKE mutant (*16*). The proposed normal permeation process is shown in the upper two panels, with Na^+ displacing Lys-1237 from its interaction with Glu-755. Mutation of selectivity filter residues is proposed to alter the interaction energy between Lys-1237 and Glu-755 of domains III and II.

tivity ring according to the proposed model. The dimensions are such that the positively charged amino group on the Lys side chain is in immediate contact with Glu-755 of domain II, with formation of a hydrogen bond or salt bridge, while Asp-400 of domain I, opposite to the Lys, could interact with Lys through a water bridge. This sort of interaction is typical of lysine in proteins (*35*). Consequently, the long chain of Lys-1237 of domain III and its two interacting carboxyls fill the space within the selectivity ring. In this model, the two carboxyls, Asp-400 and Glu-755, which are appropriate for the binding site for Na^+ ions within the selectivity filter, are already engaged by their interaction with the amino group of lysine. These interactions would be expected even if the DEKA residues were not planar, because of the flexibility of the side chains. Replacement of Lys with Ala results in removal of this block. This greatly increases the functional size of the selectivity ring opening, because the carboxyls now withdraw from the pore by electrostatic repulsion. Sun et al. (*21*) have shown that this mutation in the Na^+ channel permits permeation of bulky organic cations, including tetramethylammonium and tetraethylammonium (diameter = 8.2 Å). Consequently, it appears that normally the lysine side-chain blocks the pore to permeation by these larger cations by its interaction with the carboxyls, as illustrated in Figure 10.

The lysine side chain is also critical for selectivity of Na^+ over K^+ (*14*−*16*, *28*, *54*). Any residue substituted for Lys results in approximately equal permeability for Na^+ and K^+. This is not simply the consequence of a positive charge, because substitution with Arg fails to preserve selectivity for Na^+ with respect to K^+. Other residues in the DEKA locus appear to have smaller roles in this selectivity process. Neutralization of Asp-400 of domain I by Asn substitution markedly reduces Na^+ permeation rate (*13*, *18*), but fails to affect the selectivity of K^+ (P_K/P_{Na} = 0.03) (*15*). Neutralization of Glu-755 in domain II resulted in a modest increase in relative K^+ permeation (P_K/P_{Na} = 0.09) (*15*), although it also drastically reduces single channel conductance (*13*, *19*). Replacement of Ala-1529 by the long side chain of Glu also increased the permeability of K^+ (P_K/P_{Na} = 0.15) (*16*). The residue effects are positional, because simple exchange of positions of the Lys and Glu residues within the ring (DEKA to DKEA) further reduces selectivity (*16*). In addition, there are reports that mutations of other residues in the vestibule can affect selectivity. Both Chiamvimonvat et al. (*19*) and Tsushima et al. (*20*) have reported that substitution of Cys for Asp-1532 or Trp-1531 alter the P_K/P_{Na} ratio substantially. For Asp-1532, this is partly related to charge at that site, because restoration of charge with methanethiosulfonate ethylsulfonate tends to restore selectivity (*19*). Our studies (*44*) have failed to show a selectivity change for D1532N. Replacement of Trp-1531 with a hydrophobic residue (Ala, Phe, and Tyr) preserved selectivity (*20*), suggesting that the hydrophobic interaction we propose to be necessary to stabilize the α-helix-turn-strand of domain IV is important for the vestibule function.

Can these complex selectivity changes be understood in terms of the modeled structure (Figure 11)? In the wild-type channel with DEKA, Lys(III) forms a strong interaction with Glu(II) and interacts through a water bridge with Asp(I). In this conformation, we propose that Na^+ has sufficient energy to displace the ammonium group of Lys from its interaction with the carboxyls, but K^+ is less successful. For the selectivity process, only the close interaction between Lys(III) and Glu(II) is important. Asp(I) is needed for rapid permeation, perhaps via its negative field and hydrophilicity, but is not required for selectivity. Replacement of Glu(II) by Ala leads to interaction of Asp(I) with Lys(III) and continued block of the pore. However, this interaction has lower energy

because of the necessary water bridge, and K^+ is therefore more effective in displacing the ammonium group. Less obvious is the possible mechanism of effect of Glu in place of Ala in domain IV. Possibly, this also electrostatically destabilizes and weakens the close interaction between Glu(II) and Lys(III), so that K^+ can compete more successfully and, therefore, permeate better.

The logic described above leads to the following proposal for the normal process of selectivity for Na^+ over K^+. The normal binding site for permeation of Na^+ includes two carboxyls—Asp(I) and Glu(II). These both interact with Lys(III), and they close the selectivity ring to permeation almost entirely. Na^+ as a stronger Lewis acid is able to compete with the amino group of Lys more successfully than K^+, displacing the Lys(III) away from the carboxyls and toward Ala(IV), allowing the Na^+ ion to interact directly with one of the carboxyl groups, Glu(II) or Asp(I). Consequently, this implies a dynamic model of selectivity, with the Lys(III) side chain undergoing a conformational change for each Na^+ ion that pemeates. Selectivity is not determined by the size of the pore at the selectivity ring level but by the ability of the permeating ion to compete with the amino group of Lys. Li^+, with an ionic radius significantly less than that of Na^+ (0.6 and 0.95 Å, respectively), is also effective in displacing Lys, while K^+, Rb^+, and Cs^+ are not as effective, as predicted by the Eisenman series for a strong field site (*2*). The proposed interactions are possible because of the exact spacial relationship of the DEKA selectivity filter residues. Favre et al. (*15*) have proposed somewhat different mechanism by analogy to the two-divalent site selectivity filter of the Ca^{2+} channel (*55*, *56*). They suggest that the permeating Na^+ binds to the static selectivity filter, with the positively charged Lys amino group stabilizing the metal-binding cavity to an appropriate size. Lys(III) then acts as a second, endogenous cation, altering affinity of Na^+ binding within the pore. In both cases, it is clear that the positive charge tethered to domain III must have a large effect on the electrostatic field within the selectivity filter and on any cations in that region.

The permeability of organic cations through the selectivity filter is restricted by their capability to substitute for the water bridge to Asp-400 inside the ring (Figure 10). Removal of the water molecule without disturbing the Glu-755—Lys-1237 interaction results in the pore opening approximately 3.2×5.2 Å in size (see ref *2*). Guanidinium is small enough to fit this opening, and it can replace the water bridge between Asp-400 and Lys-1237. Despite similar size, permeability of hydroxylammonium is close to that of Na^+, whereas methylammonium is practically impermeant (*2*). The possible explanation for this difference in permeation between similarly sized molecules is that the hydroxyl group of hydroxylammonium can interact with Asp-400 and Lys-1237 simultaneously. Methylammonium is not able to form the bridge because of its hydrophobic side chain, failing to open the space in proximity to the side chain of Ala-1529 of domain IV.

Modeling Summary. We tested the idea that the P loop motif, the M1/M2 teepee motif, and the coordinates of the KcsA channel crystal structure could be applied to the voltage-gated Na^+ channel pore. The channel vestibule P loops could be constructed with the α-helix-turn-β-strand motif, preserving the characteristics of the multivalent guanidinium toxin binding sites. Local anesthetic interactions with the inner pore were used to align the S6 helical residues, and the S5 and S6 helices could then be assembled with the KcsA helical coordinates. The Na^+ channel P loop structures could then be docked into the teepee, locating the selectivity filter just external to the residues involved in the inner drug sites. In this model, the outer vestibule is formed by elements of the P loops and the S6 helices, with the S6 structures setting limits on the dimensions of the selectivity filter. Na^+ interacts directly only with the residues of the DEKA motif. The filter structure leads to the suggestion that selectivity in the Na^+ channel is normally blocked by an interaction between the amino group of lysine and the carboxyl group of domain II glutamate, with the amino group acting as a tethered cation. Selectivity is a dynamic process that results in displacement of the Lys amino group by Na^+ more successfully than by K^+. We conclude that the crystal structure and motifs of the KcsA channel are useful to interpret the structure of the voltage-gated Na^+ channel, to make predictions of exact residue locations for further mutational study.

ACKNOWLEDGMENT

We appreciate the advice of Drs. Dorothy Hanck, Akihiko Sunami, and Samuel Dudley during the development of this model.

REFERENCES

1. Doyle, D. A., Cabral, J. M., Pfuetzner, R. A., Kuo, A., Gulbis, J. M., Cohen, S. L., Chait, B. T., and MacKinnon, R. (1998) *Science 280*, 69−74.
2. Hille, B. (1992) *Ionic channels in Excitable Membrane*, 2nd ed., Sinauer, Sunderland, MA.
3. MacKinnon, R. (1991) *Nature 350*, 232−238.
4. Catterall, W. A. (1992) *Physiol. Rev. 72* (Suppl.), S15−S48.
5. Goldin, A. L. (1994) in *Handbook of Receptors and Channels* (North, R. A., Ed.) Vol. II, pp 73−112, CRC, Boca Raton, FL.
6. Guy, H. R., and Conti, F. (1990) *Trends Neurosci. 13*, 201−206.
7. Heginbotham, L., Lu, Z., Abramson, T., and MacKinnon, R. (1994) *Biophys. J. 66*, 1061−1067.
8. Lipkind, G. M., Hanck, D. A., and Fozzard, H. A. (1995) *Proc. Natl. Acad. Sci. U.S.A. 92*, 9215−9219.
9. Guy, H. R., and Durell, S. R. (1995) in *Ion Channels and Genetic Diseases* (Dawson, D., Ed.) Rockefeller University Press, New York.
10. MacKinnon, R., Cohen, S. C., Kuo, A., Lee, A., and Chait, B. T. (1998) *Science 280*, 106−109.
11. Minor, D. L., Masseling, S. J., Jan, Y. N., and Jan, L. Y. (1999) *Cell 96*, 879−891.
12. Strong, M., Chandy, K. G., and Gutman, G. A. (1993) *Mol. Biol. Evol. 10*, 221−255.
13. Terlau, H., Heinemann, S. H., Stuhmer, W., Pusch, M., Conti, F., Imoto, K., and Numa, S. (1991) *FEBS Lett. 293*, 93−96.
14. Heinemann, S. H., Terlau, H., Stuhmer, W., Imoto, W., and Numa, S. (1992) *Nature 356*, 441−443.
15. Favre, I., Moczydlowski, E., and Schild, L. (1996) *Biophys. J. 71*, 3110−3132.
16. Schlief, T., Schonherr, R., Imoto, K., and Heinemann, S. H. (1996) *Eur. Biophys. J. 25*, 75−91.
17. Penzotti, J. L., Lipkind, G. M., Fozzard, H. A., and Dudley, S. C. (1998) *Biophys. J. 75*, 2647−2657.
18. Armstrong, C., and Hille, B. (1998) *Neuron 20*, 371−380.
19. Chiamvimonvat, N., Perez-Garcia, M. T., Tomaselli, G. F., and Marban, E. (1996) *J. Physiol. (London) 491*, 51−59.
20. Tsushima, R. G., Li, R. A., and Backx, P. H. (1997) *J. Gen. Physiol. 109*, 463−480.

21. Sun, Y.-M., Favre, I., Schild, L., and Moczydlowski, E. (1997) *J. Gen. Physiol. 110*, 693−715.
22. Guy, H. R., and Seetharamulu, P. (1986) *Proc. Natl. Acad. Sci. U.S.A. 83*, 508−512.
23. Lipkind, G. M., and Fozzard, H. A. (1994) *Biophys. J. 66*, 1−13.
24. Satin, J., Kyle, J. W., Chen, M., Bell, P., Cribbs, L. L., Fozzard, H. A., and Rogart, R. B. (1992) *Science 256*, 1202−1205.
25. Kao, C. Y. (1986) *Ann. N. Y. Acad. Sci. 479*, 52−67.
26. Chou, P. Y., and Fasman, G. D. (1978). *Annu. Rev. Biochem. 47*, 251−276.
27. Schild, L., and Moczydlowski, E. (1994) *Biophys. J. 66*, 654−666.
28. Perez-Garcia, M. T., Chiamvimonvat, N., Ranjan, R., Balser, J. R., Tomaselli, G. F., and Marban, E. (1997) *Biophys. J. 72*, 989−996.
29. Hall, J., Ling, J. X., Chang, N., Lipkind, G., French, R. J., and Dudley, S. C. (2000) *Biophys. J. 78*, A143.
30. Perez-Garcia, M. T., Chiamvimonvat, N., Marban, E., and Tomaselli, G. F. (1996) *Proc. Natl. Acad. Sci. U.S.A. 93*, 300−304.
31. Chiamvimonvat, N., Perez-Garcia, M. T., Ranjan, R., Marban, E., and Tomaselli, G. F. (1996) *Neuron 16*, 1037−1047.
32. Yamagishi, T., Janecki, M., Marban, E., and Tomaselli, G. F. (1997) *Biophys. J. 73*, 195−204.
33. Efimov, A. V. (1993) *Prog. Biophys. Mol. Biol. 60*, 201−239.
34. Fozzard, H. A., and Hanck, D. A. (1996) *Physiol. Rev. 76*, 887−926.
35. Creighton, T. E. (1993) *Proteins: Structures and Molecular Properties*, 2nd ed., W. H. Freeman and Co., New York.
36. Hsu, K., Amzel, M., Tomaselli, G., and Marban, E. (1999) *Biophys. J. 76*, A82.
37. Rice, P. A., Goldman, A., and Steitz, T. A. (1990) *Proteins 8*, 334−343.
38. Volbeda, A., Lahm, A., Sakiyama, F., and Suck, D. (1991) *EMBO J. 10*, 1607−1618.
39. Banner, D. W., Bloomer, A. C., Petsco, G. A., Phillips, D. C., Pogson, C. I., and Wilson, I. A. (1975) *Nature 255*, 609−612.
40. Olsen, H. B., Ludvigsen, S., and Kaarsholm, N. C. (1996) *Biochemistry 35*, 8836−8845.
41. Ragsdale, D. S., McPhee, J. C., Scheuer, T., and Catterall, W. A. (1994) *Science 265*, 1724−1728.
42. Sunami, A., Dudley, S. C., and Fozzard, H. A. (1997) *Proc. Natl. Acad. Sci. U.S.A. 94*, 14126−14131.
43. Wang, G. K., Quan, C., and Wang, S.-Y. (1998) *Mol. Pharmacol. 54*, 389−396.
44. Chang, N. S., French, R. J., Lipkind, G. M., Fozzard, H. A., and Dudley, S. C. (1998) *Biochemistry 37*, 4407−4419.
45. Benitah, J.-P., Tomaselli, G., and Marban, E. (1996) *Proc. Natl. Acad. Sci. U.S.A. 93*, 7392−7396.
46. Benitah, J.-P., Ranjan, R., Yamagishi, T., Janecki, M., Tomaselli, G. F., and Marban, E. (1997) *Biophys. J. 73*, 603−618.
47. Li, R. A., Velez, P., Chiamvimonvat, N., Tomaselli, G. F., and Marban, E. (2000) *J. Gen. Physiol. 115*, 81−92.
48. Chahine, M., Sirois, J., Marcotte, P., Chen, L.-Q., and Kallen, R. G. (1998) *Biophys. J. 75*, 236−246.
49. Qu, Y., Rogers, J., Tanada, T., Scheuer, T., and Catterall, W. A. (1995) *Proc. Natl. Acad. Sci. U.S.A. 92*, 11839−11844.
50. Wang, G. K., Quan, C., and Wang, S.-Y. (1998) *Pfluegers Arch. 435*, 293−302.
51. Sunami, A, Lipkind, G., Glaeser, I. W., and Fozzard, H. A. (1999) *Biophys. J. 76*, A81.
52. Liu, Y., Holmgren, M., Jurman, M. E., and Yellen, G. (1997) *Neuron 19*, 175−184.
53. del Camino, D., Holmgren, M., Liu, Y., and Yellen, G. (2000) *Nature 403*, 321−325.
54. Chen, S.-F., Hartmann, H. A., and Kirsch, G. E. (1997) *J. Membr. Biol. 155*, 11−25.
55. Almers, W., and McCleskey, E. W. (1984) *J. Physiol. (London) 353*, 585−608.
56. Hess, P., and Tsien, R. W. (1984) *Nature 309*, 453−456.

BI000486W